Stability of fatigue cracks at 350°C in air and in liquid metal in T91 martensitic steel

Jean-Bernard VOGT*, Jérémie BOUQUEREL, Carla CARLE and Ingrid PRORIOL SERRE
Univ. Lille, CNRS, INRA, ENSCL, UMR 8207 - UMET - Unité Matériaux et Transformations, F-59000 Lille, France

***Corresponding author**: jean-bernard.vogt@univ-lille.fr

Abstract. The low cycle fatigue behaviour of a 9Cr1MoNbV martensitic steel has been investigated at 350°C in air and in lead-bismuth eutectic (LBE) with low and high oxygen content. Total strain controlled tests were performed from $\Delta\varepsilon_t$ = 0.40% to 1.2%. The material exhibited a pronounced cyclic softening in both environments. LBE reduced the fatigue resistance. LBE accelerated the formation of the long crack by promoting the growth of the first short cracks. A clear change in propagation mode was observed. In air, ductile fatigue striations were observed while in LBE a brittle fracture decorated by voluminous and largely spaced striations were visible. From EBSD analysis, it was concluded that in LBE, the long crack advanced quickly by repeated and discontinuous cleavage.

Keywords: fatigue crack mechanism – brittle fracture – low cycle fatigue

Nomenclature:

LME: Liquid Metal Embrittlement
LMAD: Liquid Metal Accelerated Damage
LBE: Lead Bismuth Eutectic
LCF: Low Cycle Fatigue
EBSD: Electron Back Scatter Diffraction
LOC-LBE: Low Oxygen Content Lead Bismuth Eutectic
OS-LBE: Oxygen Saturated Lead Bismuth Eutectic
EDS: Energy Dispersion Spectroscopy
IPF: Inverse Pole Figure
$\Delta\varepsilon_t$: total strain range
N_f : number of cycles to failure

1 Introduction

Thanks to the efforts targeted on the development on heat resistant steels for power plants [1] during the last decades, ferritic martensitic 9-12% Cr cannot be ignored for high temperature applications. Among them, T91 martensitic steel is a modified grade of the 9Cr1Mo steel family. It exhibits excellent combination of strength and ductility which can be achieved by control of the heat treatment. With the addition of niobium and tungsten, T91 steel is particularly chosen for application where creep resistance is required. It is therefore employed for structural components in all industrial fields working at high temperatures such as refineries or power plants including nuclear power plants. With an amount of chromium less than 10.5 wt %, the alloy cannot be classified as stainless steel and is not really designed to operate in corrosive environments as can do the 12Cr steels. Nevertheless, T91 steel has been considered as one of the materials to be possibly employed for components of accelerator driven systems (ADS) or of Gen IV nuclear reactors. These systems employ liquid metals as spallation target or as coolant. Even if the ductility of T91 steel is somewhat appreciable, it can be decreased by irradiation e.g. [2] or by long term exposure at high temperature e.g. [3]. Besides these operating conditions that affect the bulk of the material, acceleration of damage initiation by the liquid metal environment may occur as it is the case for aqueous environments e.g. [4]. Even if both aqueous medium and liquid metal can provoke degradation of the material by corrosion, mechanisms are different, and hence corrosion-deformation interaction as well. However, there are some similarities in terms of macroscopic response of materials deformed in a liquid metal and other media. A very amazing response that can exhibit a ductile material stressed in liquid metal is the so called liquid metal embrittlement (LME) or liquid metal assisted damage (LMAD). It has been shown by several authors working in the field of materials in contact with lead bismuth eutectic (LBE) that T91 steel is especially sensitive. For T91 steel, the ductile to brittle transition in LBE at 300°C is strongly influenced by the heat treatment and especially the tempering temperature [5].

Attention has already been paid since a long time on the low cycle fatigue behaviour of 9% Cr from room temperature [6] up to 600°C [7]. The cyclic response is characterized by a softening which is dependent on strain rate and test temperature. Cycling also has an impact of the stability of the microstructure. A transformation of unstable martensite lath structure to dislocation sub-grain structure by forming dislocation cell structure has been observed even at room temperature. The LCF behaviour of 9Cr1Mo steel in liquid metals has been less studied but nevertheless some results accepted by some researchers is that the fatigue life is affected by the presence of liquid metal in

comparison with air or inert environment. While the fatigue lives at 600°C are longer in liquid sodium [8] than in air, they are reduced when fatigue experiments are conducted in heavy liquid metals (Pb or Pb-Bi) [9, 10 ,11]. This decrease in fatigue resistance by liquid metals is the most observed one since it has been also reported on other 9-12%Cr martensitic steels and 316L austenitic steels fatigued in LBE [12] or in mercury [13]. The mechanisms of fatigue crack propagation of martensitic in liquid metals is however few documented except the recent work of Gong et al. [10].

The objective of the present paper is to study the LCF response at 350°C of a modified 9Cr 1Mo steel in liquid LBE by paying attention on the behaviour of short and long cracks. The strain controlled test on cylindrical polished specimen will be employed for that. Indeed, shorts cracks are those initiated from the intrusions and grown at the external surface with a size ranging between one and ten grain sizes. The long crack is the evolution of one of them evolves and propagates into the bulk. Oxygen content in LBE will considered since it reacts with iron surface to form oxide acting thus as a barrier which decreases the risk of LME.

2 Materials

The material (T91 steel) was supplied in the frame of the European project MatISSE as rolled plates with 15 mm in thickness. The material was heat treated by the supplier at 1100°C for 15 minutes followed by water cooling and a subsequent tempering for 45 minutes at 770°C and then air cooling.

The chemical composition of the studied material is given in Table 1.

Table 1: chemical composition of the investigated T91 steel (wt %)

C	**Cr**	**Mo**	**Nb**	**V**	**P**	**S**	**Ni**	**Al**	**Cu**
0.1025	8.99	0.89	0.06	0.21	0.021	0.0004	0.11	0.0146	0.06
Si	**Sn**	**As**	**Ti**	**Mn**	**W**	**Pb**	**B**	**N**	**Fe**
0.22	0.004	0.008	0.0034	0.38	0.01	< 10ppm	< 1ppm	0.0442	Bal.

After metallographic preparation and etching with Villela solution (100 mL ethanol, 5 mL chlorhydric acid, 1 g picric acid), the microstructure appeared to be fully tempered martensitic with an average prior austenitic grain size of 20 ± 5 µm (Fig. 1a). This was confirmed by X-ray diffraction (XRD) and electron back scatter diffraction (EBSD) analysis. Note that a martensitic structure is

hierarchically organized. The prior austenite grain is divided into packets which comprise blocks of martensite laths (Fig. 1b). Therefore, the material is rich in interfaces.Intensive analysis of precipitates has not been undertaken for the present material of this paper. As documented by Gong et [10] for the same material, including elaboration process, chemical composition and heat treatment, it is expected to find $M_{23}C_6$ type precipitates at interfaces such as prior-austenite grain boundaries and lath boundaries.

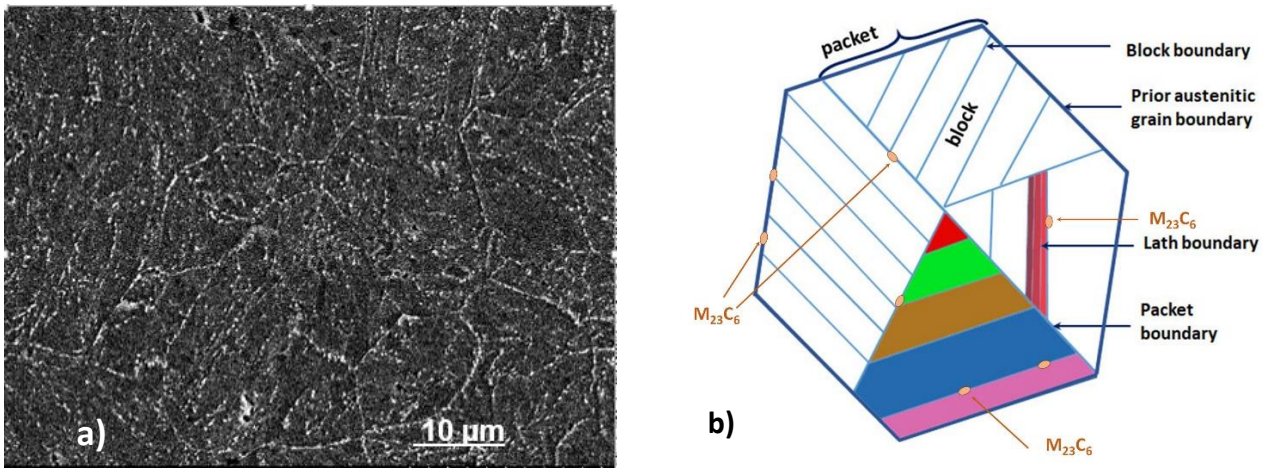

Fig. 1. a) SEM micrograph of the material before fatigue testing and b) schematic illustration of the hierarchical microstructure

The material had an average hardness value of 220 ± 5 HV.

3 Experimental details

Low cycle fatigue (LCF) tests were carried out at 350°C in air, in oxygen saturated lead-bismuth eutectic (OS-LBE) and in low oxygen content LBE (LOC-LBE). The chemical composition of LBE was 45 wt% Pb and 55 wt% Bi. To perform the tests in LBE, the fatigue specimen was immersed into a small reservoir containing the OS-LBE or the LOC-LBE and then installed onto the machine grips. For the tests in LOC-LBE, an isolating cell made of glass inside which air was first removed and then Ar-3.5% H_2 introduced was surrounded the reservoir with the specimen. For tests in air or in OS-LBE, no special care of the environment was paid.

LCF tests were carried out using a servo-hydraulic Schenk machine with a load capacity of 250 kN under total axial strain control $\Delta\varepsilon_t$ ranging from 0.40% to 1.2%. A fully push pull mode (R_ε = -1), a triangular waveform and a constant strain rate of 4.10^{-3} s^{-1} were used. In the present study, the strain at the gauge section has not been measured directly by fixing an extensometer directly on the specimen. Two offset bars were provided above and below the reservoir and were used to fix the extensometer. A calibration step was initially performed to convert the strain measured outside the specimen into the real strain at the gage part.

The specimens were smooth and cylindrical with a gauge length of 10 mm and a gage diameter of 6 mm. In order to avoid effects due to the roughness of the surface and to residual stresses developed during the machining, the sample surface was carefully electro polished before fatigue tests.

A similar method as described in reference [14] has been employed for the removing of oxygen from the received LBE. First, a LBE ingot was molten in an external furnace and transferred in the liquid state into a first tank for a primary purification. The superficial oxide layer was removed under argon flow to avoid contamination of the system. The tank was then locked and preconditioning of the LBE was performed by bubbling an Ar-3.5%H_2 gas mixture for a determined duration through the liquid metal at 550°C. Then, the preconditioned LBE was transferred by a tilted heating tube to another tank for an advanced purification. This tank was vacuumed and then washed with Ar-3.5%H_2 gas mixture before the transfer of LBE. The preconditioned LBE was as well deoxygenised by bubbling the Ar-3.5%H_2 gas mixture in the liquid metal and the oxygen content was measured with a BiO/Bi sensor. This allowed decreasing the oxygen content up to 10^{-8} wt % at 450 °C. The entire description of the procedure for cleaning LBE from oxygen can be found in [14].

The fatigue life N_f, is defined as the number of cycles needed for a 25% drop in the tensile stress taking as a reference the (pseudo) stabilized hysteresis loop.

Crack initiation sites and fracture surfaces identification of fatigued specimens were performed by SEM observations using a FEI Quanta 400 equipment.

Deep investigations of the microstructure along the crack lips were performed according to EBSD. Some fatigue specimen were fatigued until a long crack that has propagated into the bulk and stopped before fracture into two pieces of the specimen. The latter was then gently cut in a plan parallel to the specimen axis and then polished mechanically with SiC paper of a grade up to 1200 grit paper, then with 9, 3 and ¼ µm diamond pastes. The final mechanical polishing consisted of prolonged mechanical polishing with colloidal silica. SEM-EBSD analysis were carried out on a JEOL 7800F FEG-SEM fitted with an Oxford Instruments EDS/EBSD system. A Nordlys Max²CCD

camera was used for pattern acquisition and data were recorded using Oxford Instruments Aztec software. The analyses were carried out using Oxford Instruments Channel 5 commercial software. Acquisition parameters were set to reach an angular resolution of about 0.16° [15, 16]. As the martensite T91 steel exhibits a quite fine microstructure, a step size for acquisition of 70 nm was chosen for all the acquired maps.

4 Results

4.1 Stress response to strain cycling

The evolution of the stress amplitude with the number of cycles is given in Fig. 2.

Apart from the test performed at $\Delta\varepsilon_t$ = 0.4%, the material cycled at 350°C presents a strong tendency to softening at the beginning of cycling and then at a moderate rate. Then the fall of the stress is more moderate. Finally a marked decrease of the stress amplitude occurs that is related to the propagation of a macroscopic crack into the bulk just before the final failure.

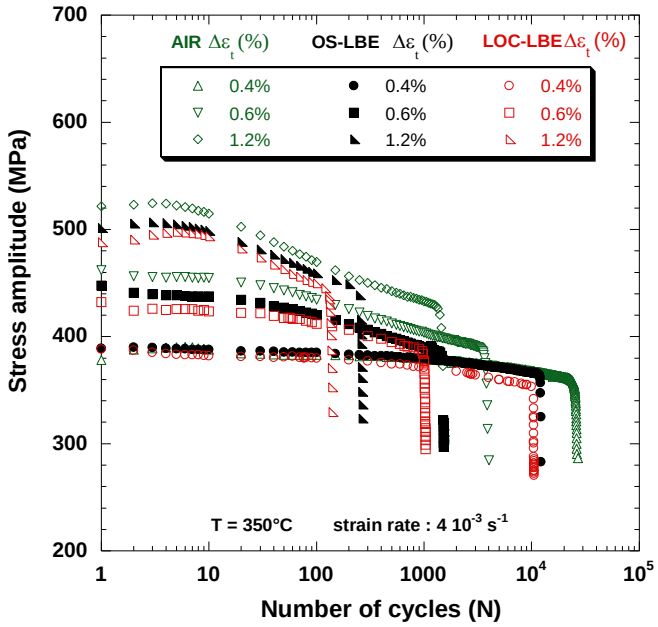

Fig. 2. Evolution of the stress amplitude with the number of cycles of T91 tested at 350°C in air, in oxygen-saturated LBE (OS-LBE) and low oxygen content LBE (LOC-LBE)

The same overall behaviour is observed that the material was cycled in air or in LBE except for the final decrease in the stress amplitude which is affected by the liquid metal. Note that the amount

and the duration of the initial softening clearly depend on the applied strain range only. As well a tendency to start with cyclic hardening seems to occur if the strain range is at least 1.2%.

4.2 Effect of LBE on fatigue crack initiation resistance

The evolution of the plastic strain variation and of total strain variation as a function of the number of cycles to failure is plotted Fig. 3a and Fig.3b respectively. The detrimental effect of LBE on the fatigue resistance of T91 steel in comparison with tests performed in air is clearly again confirmed. The results of this present study corroborates the global negative impact of heavy liquid metals on fatigue resistance of alloyed structural steels as mentioned in the introduction. Fig. 3 also points out the effect of LBE chemistry. For tests performed in LOC-LBE, the fatigue lives can be grouped in two sets of data as shown by the rectangles in the figures. The first set of data does not exhibit any difference with those obtained in OS-LBE. For the second set of data, fatigue lives in LOC-LBE are shorter than those in OS-LBE, and the gap is especially marked as the strain range is low. For nearly the same testing conditions, the same observation was given by Gong et al [17].

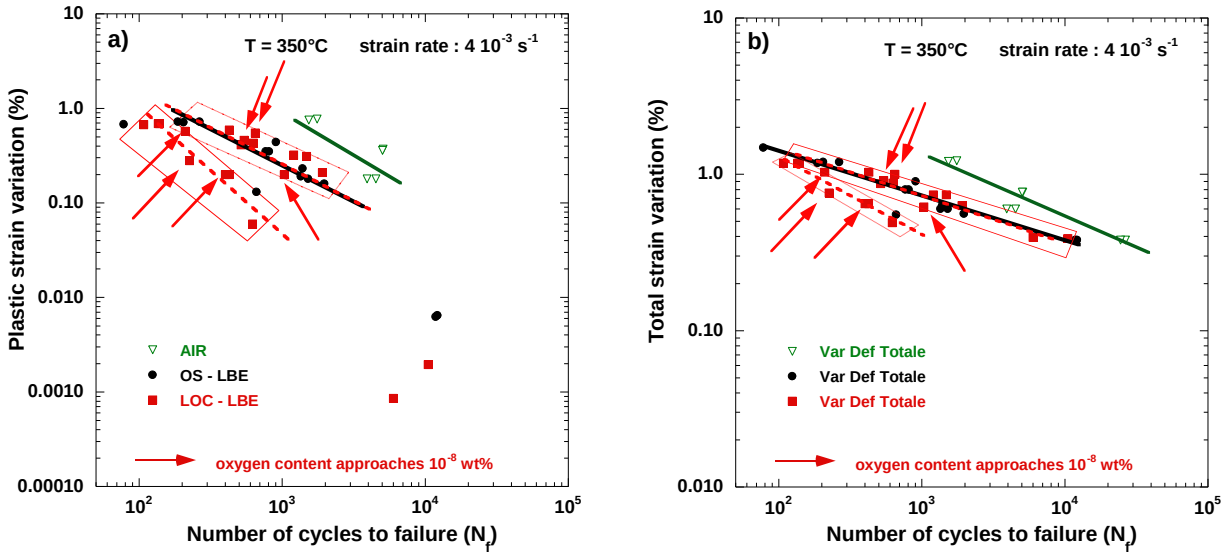

Fig. 3. Evolution of a) the plastic strain variation and b) of the total strain variation with the number of cycles to failure of T91 tested at 350°C in air, in oxygen-saturated LBE (OS-LBE) and low oxygen content LBE (LOC-LBE)

4.3 Effect of LBE on fatigue crack propagation resistance

Normally, the study of fatigue crack propagation is performed by using pre-cracked specimens in order to connect the fatigue crack velocity da/dN to the cyclic stress intensity factor ΔK. This could

not have been performed. However, the final part (the last 10 percent of the fatigue life) of the curves stress amplitude-number of cycles was analysed for that by introducing the rate of decrease (R.D.), calculated as follow:

$$\text{R.D.} = \frac{1}{N_{25\%} - N_{5\%}}$$

where $N_{25\%}$ and $N_{5\%}$ are the number of cycles correspond to a 25% drop in the tensile stress and to a 5% drop in the tensile stress respectively.

The result is reported in Fig. 4. The resistance to fatigue crack propagation changes with the environment in the same way at the resistance to fatigue crack initiation. Fig. 4 shows that the long crack propagates much faster in LBE than in air up to a factor of ten.

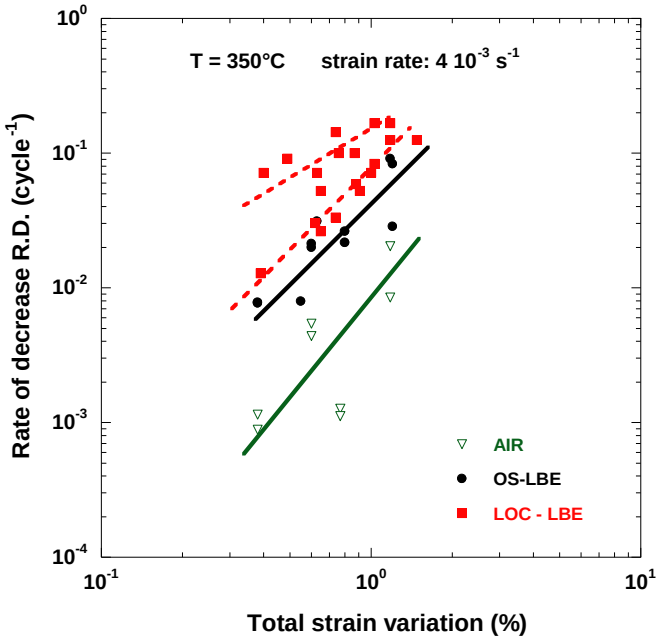

Fig. 4. Crack velocity of the long crack versus the total strain range of T91 steel fatigued in air and LBE at 350°C expressed with the rate of decrease (see the text for the definition)

The chemistry of LBE also affects the velocity of the crack. Decreasing the oxygen content in LBE resulted in an increase in the crack velocity. However, as for crack initiation, the data can be arranged in two groups, the one with a velocity slightly higher than the velocity in oxygen saturated LBE and another one with much higher velocities especially when the material was cycled at low strain range.

4.4 Short crack analysis

Fatigue specimen were cut transversally in order to appreciate the number and the depth of the short cracks. After cutting, the specimen were polished to have a mirror surface and then were etched with the Villela etchant. After fatigue in air, it was possible to observe on the transverse cross sections a lot of short cracks of different lengths (Fig. 5a) and with a quantity increasing with the strain range.

After fatigue in LBE, the number of short cracks was considerably reduced. In OS-LBE, it was very difficult to observe any short crack so that it can be considered that the specimen contained only the main crack (Fig. 5b). In LOC-LBE, the situation was a little bit different since the long crack was accompanied by a few but noticeable short cracks the number of which was increased with the applied strain range (Fig.5c).

The strain range had a noticeable effect on the density of short cracks in air, i.e. the density increased with the increasing strain range.

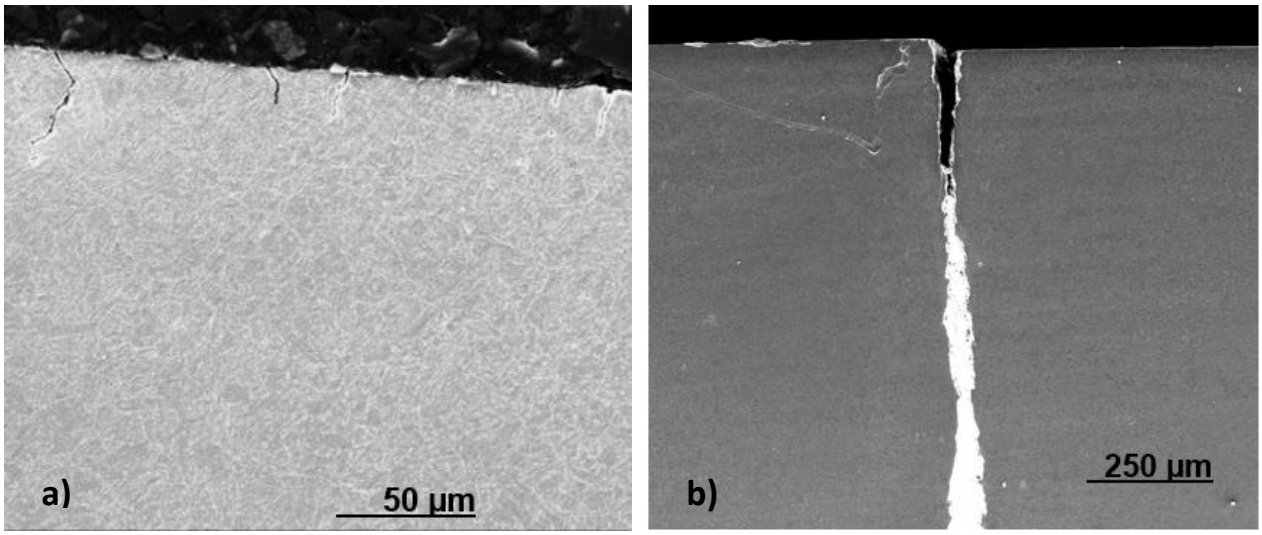

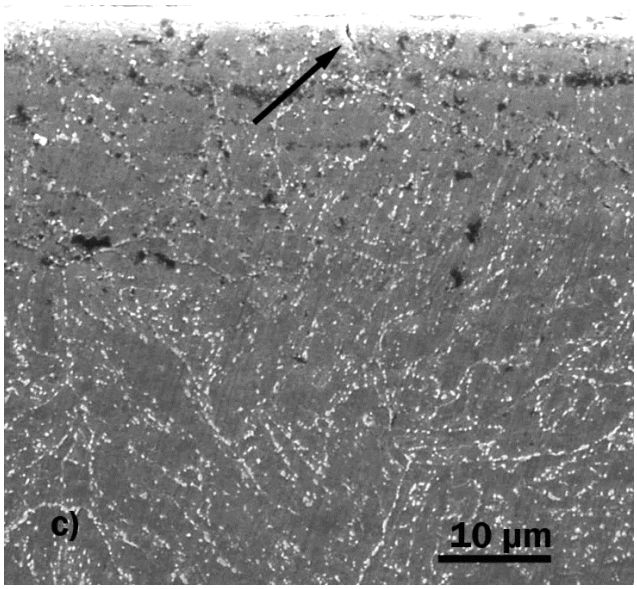

Fig. 5. Observation of short cracks in T91 steel fatigued in air at 350° C in a) air at $\Delta\varepsilon_t$= 1.2% , b) OS-LBE at $\Delta\varepsilon_t$= 0.6% and c) LOC-LBE at $\Delta\varepsilon_t$= 0.6%

4.5 Long crack analysis

The long crack morphology was first observed directly on the gage length of the specimen. After fatigue in air, the tip of the crack was accompanied by a rough zone. The rough aspect tended to vanish gradually the observation left the crack tip. However, even at 1 mm from the crack tip, the plastic deformation was still visible for the test performed at $\Delta\varepsilon_t$= 1.2%. By contrast, after fatigue in LBE, the crack path appeared more serrated without any roughness on the lips.

The most striking difference between cycling in air and in LBE (both OS and LOC) was the fracture surface morphology. In air, in agreement with the short crack distribution, the fracture surface contained multiple crack initiation sites from which several cracks propagate by fatigue in the bulk and a final fracture due to monotonic loading (Fig. 6a). Fatigue striations could be observed by SEM (Fig. 7a). The fracture surfaces of specimen cycled in LBE are totally different. First, the fracture surface was very flat and contained a single initiation site from which the crack propagated by cyclic loading. The final fracture occurred by pure tensile loading. On the fracture surface related to cyclic loading, it was possible to see at very low magnification, and even with the naked eye, curved striations (Fig. 6b). For a given strain range, the distance between two striations increased as long as the crack advanced in the bulk.

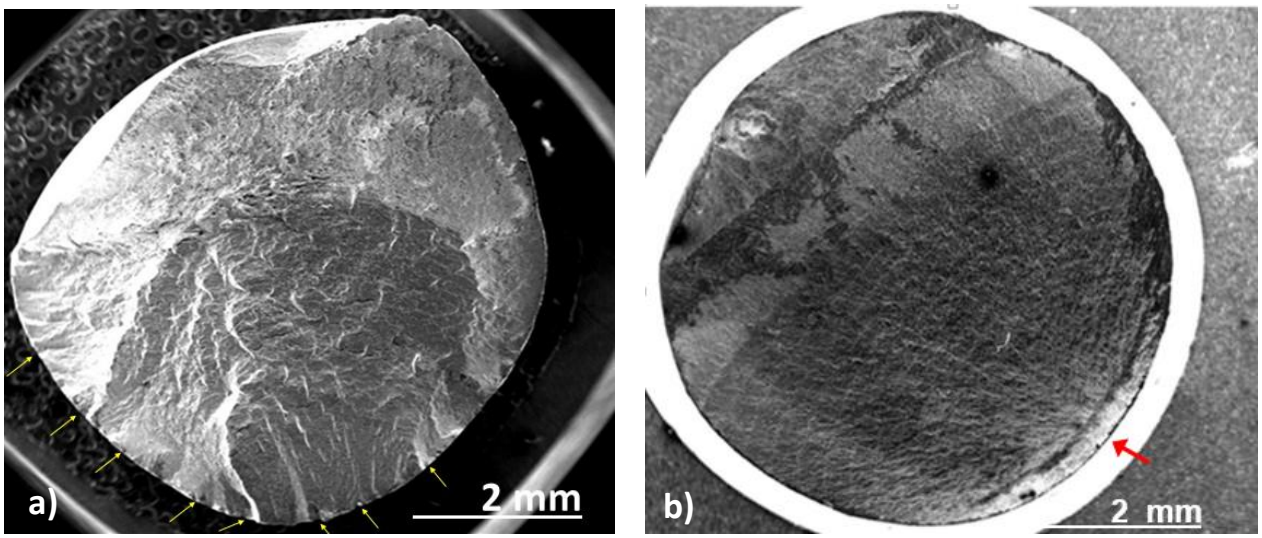

Fig. 6. Macroview of the fracture surface of T91 steel fatigued at 350° C and $\Delta\varepsilon_t$= 1.2% a) in air with yellow arrows indicating multiple site crack initiation sites and b) in LBE with the red arrow indicating the single crack initiation

At higher magnification, SEM observations pointed out transgranular brittle fracture (Fig. 7b).

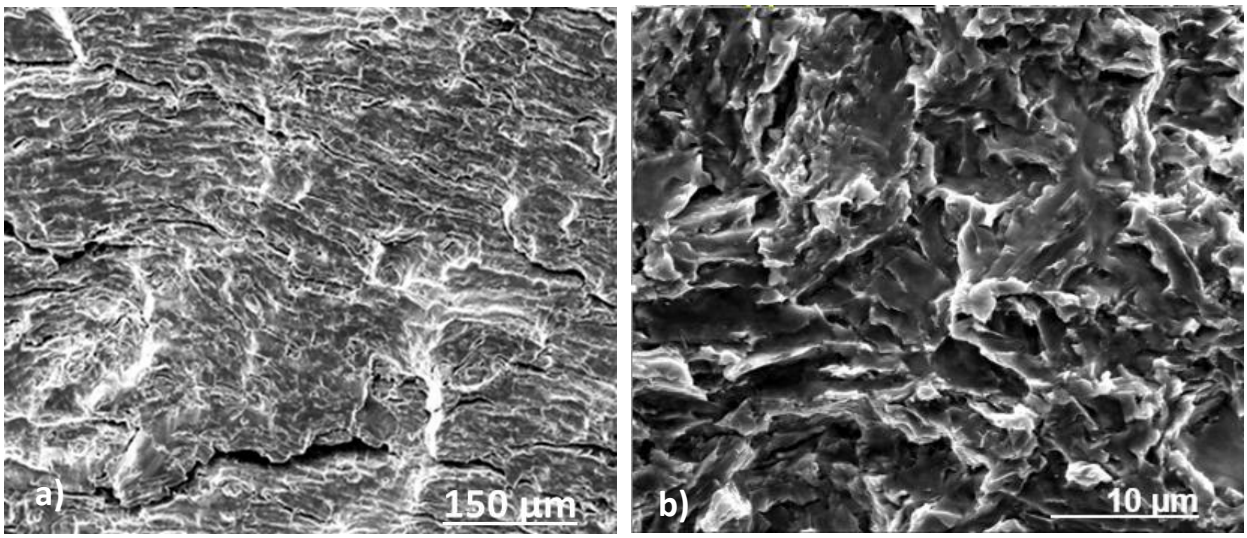

Fig. 7. SEM micrographs of the fracture surfaces of T91 steel fatigued at 350° C and $\Delta\varepsilon_t$= 1.2% showing a) ductile striations in air and b) brittle fracture between two striations in OS-LBE

In order to link the observed differences in initiation and propagation of fatigue cracks to the microstructure evolution, SEM-EBSD analysis were performed on specimen fatigued in air and in LBE at $\Delta\varepsilon_t$ = 1.2%. When the long crack was supposed to propagate in the bulk, then the test was stopped, the specimen removed and cut along the loading direction.

EBSD patterns were acquired far away from the crack to have a reference state, on the crack lips very close to the external surface, at 2.5 mm from the external surface and very near the crack tip. For the specimen fatigued in air, the inverse pole figures (IPF) revealed that the crack lips were decorated by a continuous raw of misoriented fine grains in the very first micrometres of the material adjacent to the fracture surface (Fig. 8). The grains were highly misoriented and had a grain size ranging from 0.25 µm to 0.5µm.

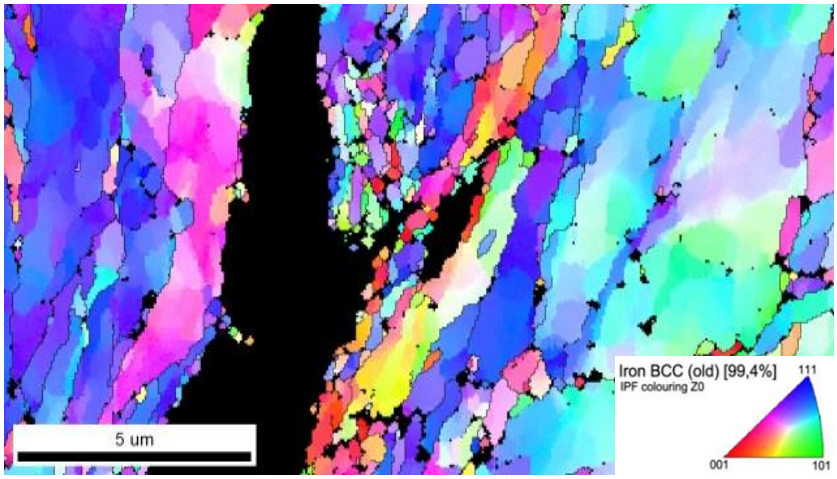

Fig. 8: IPF acquired near the crack tip in T91 fatigued in air at 350° C and $\Delta\varepsilon_t$= 1.2%

This was not observed for the specimen failed in LBE except at some spots where small groups of misoriented fine grains similar to those observed in the specimen fatigued in air could be observed (Fig. 9).

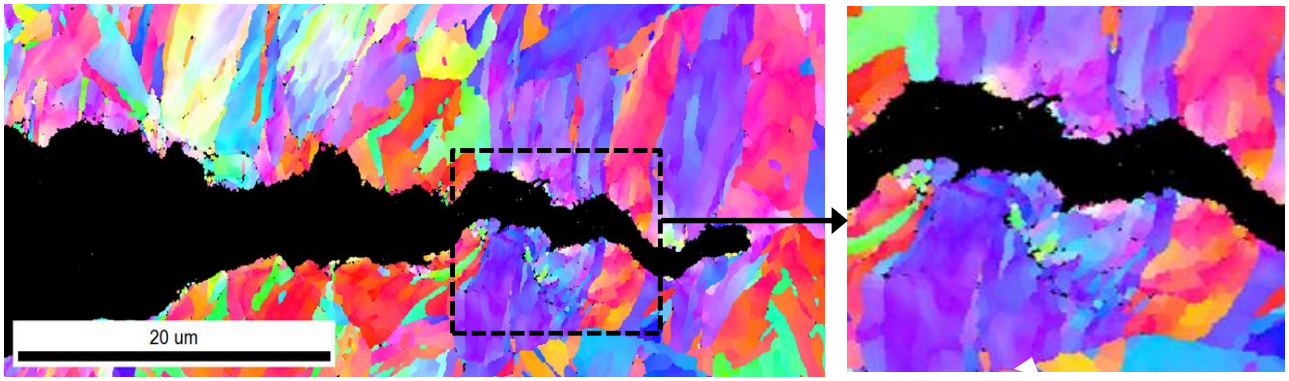

Fig. 9: IPF acquired near the crack tip in T91 fatigued in LBE at 350° C and $\Delta\varepsilon_t$= 1.2%

5 Discussion

The present investigation performed on T91 steel shows a conventional response typical of martensitic steel i.e. a cyclic softening. This is in accordance with the microstructure resulting from the heat treatment which produced and arranged a high density of dislocations. Annihilation can explain the softening and since it is a bulk effect, there is no reason why the presence of LBE should modify the response. Though martensitic steels have a multi-scaled microstructure, cyclic plasticity results in slip bands emergence at the external surface and in the formation of intrusion-extrusion pairs [18, 19]. Extrusions form first, and then intrusions at interfaces of the microstructure [18]. The latter are preferential sites for short crack initiation and their developments are sensitive to the presence of the environment. $M_{23}C_6$ precipitates have not been identified to play any major role in crack initiation and crack propagation.

The classical mechanism suggested for the transition of short cracks to long crack in air for non-complex microstructure materials can basically considered. Usually as for simple microstructure materials (single phased as copper, 316L austenitic stainless steel), the barrier arresting the short crack advance is the grain boundary. For complex microstructure materials as martensitic steels, the barriers and the crack paths are of different nature according to the loading conditions such as stress values [20]. For martensitic steels, Koschelle et al [20] have shown that prior austenitic grain boundaries and block boundaries appears as barriers for short crack propagation in the high cycle fatigue and very high cycle regimes. It is therefore reasonable to consider that the very first short cracks with a dimension of a grain or block size are hindered by the presence of boundaries which can be overcome after a given number of cycles. The crack extension proceeds by crystallographic growth and may again be delayed by other boundaries as its length reached three or four grain sizes. Longer microcracks (up to ten grain sizes typically) can eventually form by the coalescence of the shorter cracks and finally, only a very few of them propagated into the bulk perpendicularly to the stress axis.

The difference in short crack densities in specimen either cycled in air or in LBE shows that atoms of the liquid metal provided a driving force for them to overcome the structural barriers. The presence of very small microcracks in specimen fatigued in LOC-LBE as compared with OS-LBE prove that the crack instability is not only dependent upon the short crack length and the stress value but also depends upon the wettability of the intrusion tip.

The presence of fatigue striation in specimen fatigued in air is a clear indication that the crack propagated in a ductile manner. The very small distance between striations suggests that the crack

extension is slow and involves plastic deformation during tensile and compressive phase of the loading signal. The mechanism of crack advance in air is very conventional and a brief summery will help for the effect of LBE. Under a tensile loading of a little open crack (Fig. 10a), plastic deformation triggers at the tip (Fig. 10b) and becomes more and more intensive as the loading is increased, activating all available dislocations sources (Fig. 10c) and blunting the tip. By reversing the load signal, the blunted tip is sharpened and the successive blunting- resharping process leads to striations with a slow crack advance (Fig. 10d).

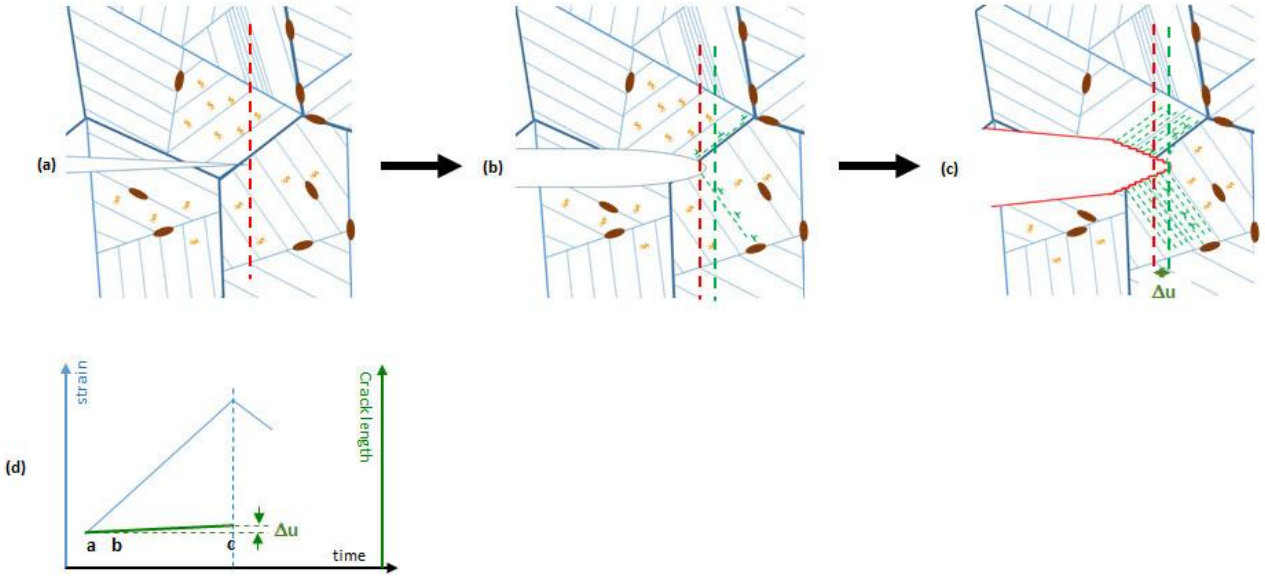

Fig. 10: Fatigue crack advance mechanism of T91 steel in air at 350°C

The new fine grains observed by EBSD along the crack lips result from a mechanical recrystallization process. Indeed, very strong activity of cyclic plasticity confined in the very first blocks adjacent produces a high density of dislocations which organize into cells of more and more intense misorientation that they become fine grains.

In LBE, the large distance between striations indicates that the crack advanced rapidly. And this is in good agreement with the observations of brittle transgranular fracture. The main difference between the two investigated environments is the form of the phase which is gaseous for tests in air and liquid for tests in LBE. The question of wedge effect and the related consequences on crack closure and crack growth rate may arise. Nevertheless, it reasonable to exclude or at least minimize this effect since a liquid may escape from the crack and annihilate any effect as opposed to solid

particles. Moreover, if any effect of wedge effect should occur, it preferentially would have an effect at rather low cyclic stress intensity factor which is not the case for the considered crack of the paper. Therefore, the modification of fracture mode between fatigue in air and fatigue in LBE is a simple appearance of LME. There are several explanations and models for LME. In our situation, the brittle fracture theory proposed by Stoloff and Johnson [21] & Westwood and Kamdar [22] and based on the weakening of inter-atomic bonds by the liquid metal atoms at the crack sounds well. LME occurrence requires an actual wetting between atoms of the liquid metal and the steel. This can be not encountered if the crack tip is not wetted due to capillarity. However, EDX analysis of the crack tip after fatigue in LBE clearly showed that the liquid metal reached the very crack tip (Fig. 11).

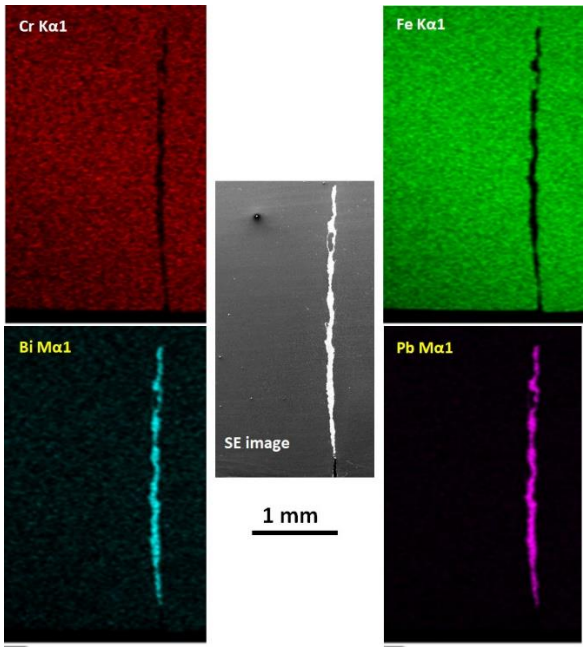

Fig. 11: Secondary electron image showing a long crack in T91 fatigued at $\Delta\varepsilon_t$ = 0.6% in OS-LBE at 350°C and EDS X-ray mapping showing the entire filling of Pb and Bi of the crack tip

Another reason for the non-wetting is the presence of an oxide film. In the present experiments, LBE was oxygen saturated which means that even if fresh surface formed in the LBE, dissolved oxygen can react with the fresh steel to form an oxide film. Therefore as for fatigue in air, under a tensile loading of a little open crack (Fig. 12a), the latter fills up with liquid LBE at the same time as plastic deformation triggers at the crack tip (Fig. 12b). The emerging steps of fresh material tend to react with oxygen since the very first moment of the tension loading but the very thin layer

of oxide is destroyed by the emerging dislocations. Even if the deoxidized surface is small, it allows adsorption of LBE atoms and then a decrease of the inter-atomic bond strength and a promoted localized shear. Indeed, beside a brittle fracture promoted by liquid metal, adsorption also affects the nucleation of dislocations [23]. Moreover, it has been shown that oxygen in the liquid LBE can drive the Pb atoms to enter the lattice along the channels formed in the cracked oxide [24]. Brittle fracture initiates and propagates along all types of interfaces such as lath interfaces, block interfaces, packet interfaces and martensitic grain boundaries in agreement with the findings of Auger et al [25]. Brittle fracture propagation through lath or packet is not excluded but due to the size of these microstructural items, it is difficult to decide. If the crack tip is actually wetted as the liquid fills up the crack, then the crack advances in a brittle manner until the maximum of loading (Fig. 12c and 12 c''). No change in the grain size was observed. Upon reversing the strain signal, the crack starts closing and leaves a mark. During brittle propagation of the crack, a more resistant oxide layer can form and behaves as a shield against adsorption of LBE atoms. The crack temporarily stops. Thereby, plastic deformation triggers at the tip (Fig. 12c'), dislocations sources activate and dislocations accumulate at the oxide film. A very small sized zone is enough heavily deformed to recrystallize. When the stress concentration is high enough to break the oxide layer, a breach forms in which LBE gets into, and in turn provides all the conditions for brittle crack propagation. In comparison with the previous situation, the crack velocity is high but discontinuous and resembles a cyclic cleavage (Fig. 12d).

Though EBSD experiments have not yet been performed on T91 fatigued in LOC-LBE, it is expected to observe the mechanism described by Fig. 12abc'. However, it is not excluded to observe the mechanism described Fig. 12 abc''c'. This is suggested by the crack velocity diagram of Fig. 4. Two regimes were observed and can be associated to the one or to the other mechanism. Indeed, even if the average amount of oxygen atoms is low, cluster of oxygen atoms can form locally which may oxide the plasticity steps.

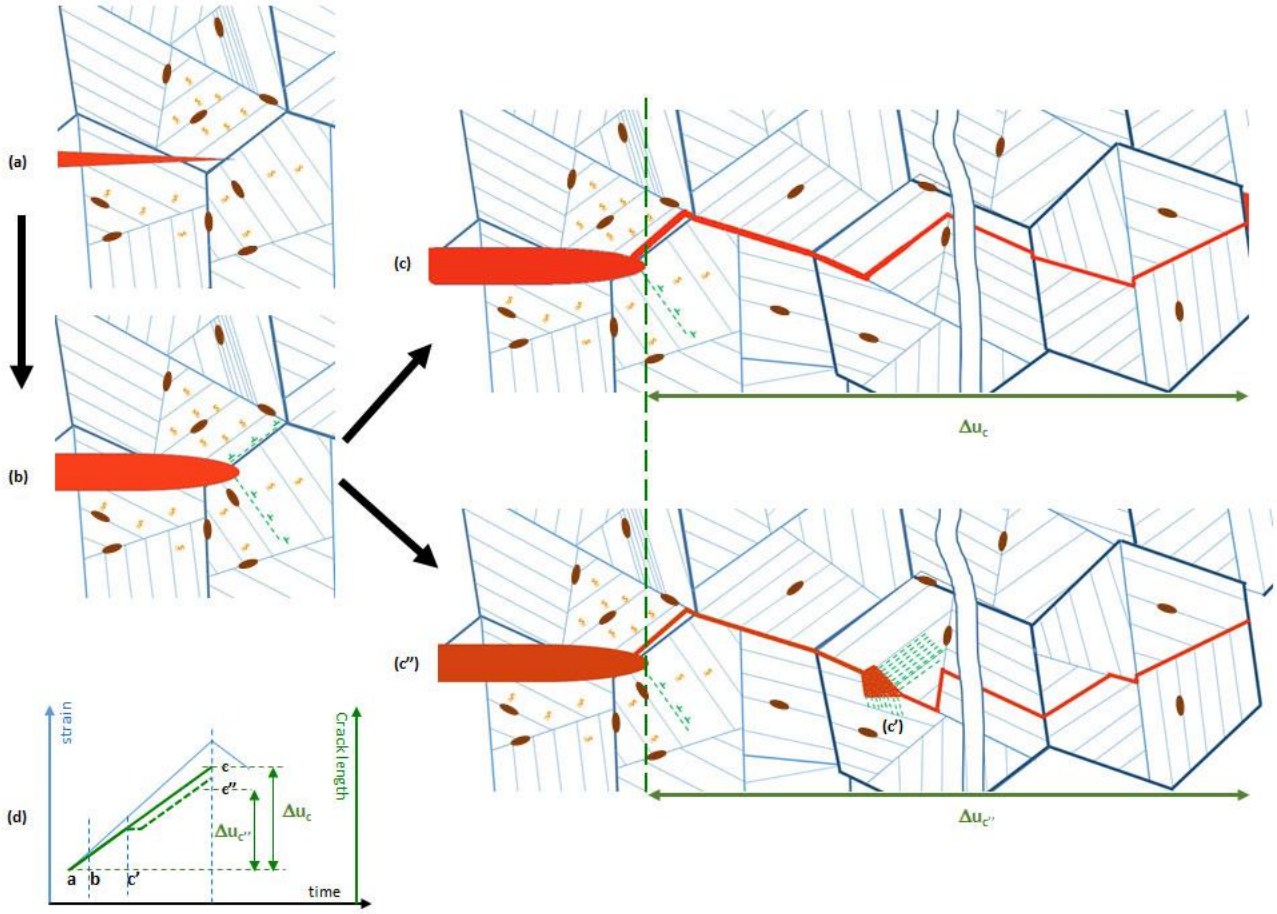

Fig. 12. Fatigue crack advance mechanism of T91 steel in LBE at 350°C

6 Conclusions

The fatigue behaviour of the T91 steel has been investigated at 350°C in air and in liquid lead-bismuth eutectic (LBE) with low and saturated oxygen content. Attention has been paid on the stability of the long crack according to the environment.

The main conclusions are:

- T91 steel softens during cycling all the more the applied strain range is high but independently of the environment
- The resistance to fatigue crack initiation is decreased in LBE in comparison with air
- Fatigue lives in low oxygen content LBE were sometimes either of the same order or much lower as those in oxygen saturated LBE
- Fatigue crack propagation rate is increased in LBE in comparison with air

- Fatigue crack propagation rate in low oxygen content LBE was sometimes either of the same order or much higher as those in oxygen saturated LBE
- Fracture surfaces contained ductile striations after tests in air but were of brittle aspect after tests in LBE
- Rapid propagation by cleavage can be momently stopped if oxygen atoms accumulate in LBE at the crack tip

Acknowledgements

The work was partly funded by the European Atomic Energy Community's (Euratom) Seventh Framework Programme FP7/2007-2013 under Grant agreement no. 604862 (MatISSE project).
Ing. J. Golek and D. Creton are acknowledged for their assistance in the experimental work.
The SEM and TEM national facility in Lille (France) is supported by the Conseil Regional des Hauts-de-France and the European Regional Development Fund (ERDF).

References

[1] Masuyama F. History of power plants and progress in heat resistant steels. ISIJ Int. 2001;41: 612-625. https://doi.org/10.2355/isijinternational.41.612

[2] Dai Y, Henry J, Tong Z, Averty X, Malaplate J, Long B. Neutron/proton irradiation and He effects on the microstructure and mechanical properties of ferritic/martensitic steels T91 and EM10. J. Nuc. Mater. 2011;415: 306-310. https://doi.org/10.1016/j.jnucmat.2011.04.029

[3] Blach J, Falat L, Ševc P. Fracture characteristics of thermally exposed 9Cr–1Mo steel after tensile and impact testing at room temperature.
https://doi.org/10.1016/j.engfailanal.2008.09.003

[4] El May M, Saintier N, O. Devos O, A. Rozinoer A. Effect of Corrosion on the Low-cycle Fatigue Strength of Steels used in Frequent Start-up Power Generation Steam Turbine. Proc. Eng. 2015;133: 528-534. https://doi.org/10.1016/j.proeng.2015.12.626

[5] Serre I, Vogt J.-B. Heat treatment effect of T91 martensitic steel on liquid metal embrittlement. J. Nucl. Mater. 2008;376: 330-335. https://doi.org/10.1016/j.jnucmat.2008.02.018

[6] Guguloth K, Sivaprasad S, Chakrabarti D, Tarafder S. Low-cycle fatigue behavior of modified 9Cr–1Mo steel at elevated temperature. Mat. Sci. Eng. 2014;A604: 196–206. https://doi.org/10.1016/j.msea.2014.02.076

[7] Verma P, Santhi Srinivas N.C, Singh S.R, VakilSingh. Low cycle fatigue behavior of modified 9Cr–1Mo steel at room temperature. Mat. Sci. Eng. 2016;A652: 30-41. https://doi.org/10.1016/j.msea.2015.11.060

[8] Kannan R, Sandhya R, Ganesan V, Valsan M, Bhanu Sankara Rao K. Effect of sodium environment on the low cycle fatigue properties of modified 9Cr–1Mo ferritic martensitic steel. J Nuc. Mater. 2009;384: 286–291. https://doi.org/10.1016/j.jnucmat.2008.11.036

[9] Verleene A, Vogt J.B , Serre I, Legris A. Low cycle fatigue behaviour of T91 martensitic steel at 300 °C in air and in liquid lead bismuth eutectic. Int. J. Fatigue 2006;8: 843–851. https://doi.org/10.1016/j.ijfatigue.2005.11.003

[10] Gong X, Marmy P, Lin Qing, Verlinden B, Wevers M, Seefeldt M. Temperature dependence of liquid metal embrittlement susceptibility of a modified 9Cr-1Mo steel under low cycle fatigue in lead-bismuth eutectic at 160-450°C, J Nuc. Mater. 2016;468: 289-298. https://doi.org/10.1016/j.jnucmat.2015.06.021

[11] Kalkhof D, M. Grosse M. Influence of PbBi environment on the low-cycle fatigue behavior of SNS target container materials. J Nuc. Mater. 2003;318: 143–150. https://doi.org/10.1016/S0022-3115(03)00015-1

[12] Naoe T, Zhihong Xiong, Futakawa M. Gigacycle fatigue behaviour of austenitic stainless steels used for mercury target vessels. J Nuc. Mater. 2016;468: 331-338. https://doi.org/10.1016/j.jnucmat.2015.07.040

[13] Tian H, Liaw P.K, Strizak J.P, Mansur L.K. Fatigue properties of type 316LN stainless steel in air and mercury. J Nuc. Mater. 2005;343: 134–144. https://doi.org/10.1016/j.jnucmat.2005.03.019

[14] Ye C, Vogt J.-B, Proriol Serre I. Liquid metal embrittlement of the T91 steel in lead bismuth eutectic: The role of loading rate and of the oxygen content in the liquid metal. Mat. Sci. Eng. 2014;A608: 242–248. https://doi.org/10.1016/j.msea.2014.04.082

[15] Thomsen K, Schmidt N.H, Bewick A, Larsen K, Goulden J. Improving the Accuracy of Orientation Measurements using EBSD. Microsc. Microanal. 2013;19: 724–725. DOI: https://doi.org/10.1017/S1431927613005618

[16] Goulden J, Bewick A. The Application of the AZtec EBSD System to the Study of Strain in the SEM. Microsc. Microanal. 2016.22: 18–19. DOI: https://doi.org/10.1017/S1431927616000945

[17] X. Gong, P. Marmy, B. Verlinden, M. Wevers, M. Seefeldt. Low cycle fatigue behavior of a modified 9Cr–1Mo ferritic–martensitic steel in lead–bismuth eutectic at 350 °C – Effects of oxygen concentration in the liquid metal and strain rate. Corr. Sci. 2015;94: 377 – 391. https://doi.org/10.1016/j.corsci.2015.02.022

[18] Seidametova G, Vogt J.B, Proriol Serre I. The early stage of fatigue crack initiation in a 12%Cr martensitic steel. Int. J. Fatigue 2018;106: 38–48. https://doi.org/10.1016/j.ijfatigue.2017.09.006

[19] Batista MN, Marinelli MC, Hereñú S, Alvarez-Armas I. The role of microstructure in fatigue crack initiation of 9–12%Cr reduced activation ferritic–martensitic steel. Int. J. Fatigue 2015;72:75–79. https://doi.org/10.1016/j.ijfatigue.2014.11.006

[20] Koschella K and Krupp U. Investigations of fatigue damage in tempered martensitic steel in the HCF regime. Int. J. Fatigue 2019;124: 113-122. https://doi.org/10.1016/j.ijfatigue.2019.02.050

[21] Stoloff N.S, Johnston T.L. Crack propagation in a liquid metal environment. Acta. Metal. 1963;11: 251-256. https://doi.org/10.1016/0001-6160(63)90180-9

[22] Westwood A.R.C,Kamdar M.H. Concerning liquid metal embrittlement, particularly of zinc monocrystals by mercury. Philos Mag 1963;8: 787-804. https://doi.org/10.1080/14786436308213836

[23] Lynch S.P. Environmentally assisted cracking: Overview of evidence for an adsorption-induced localised-slip process. Acta. Metall.1988;36: 2639-2661. https://doi.org/10.1016/0001-6160(88)90113-7

[24] Proriol Serre I, Vogt J.-B, Nuns N. ToF-SIMS investigation of absorption of lead and bismuth in T91 steel deformed in liquid lead bismuth eutectic. Applied Surf. Sci. 2019;471: 36-42. https://doi.org/10.1016/j.apsusc.2018.11.209

[25] Auger T, Hémery S, Bourcier M, Berdin C, Martin M, Robertson I. Crack path in liquid metal embrittlement: experiments with steels and modelling, Frattura ed Integrità Strutturale. 2016;35: 250-259. DOI https://doi.org/10.3221/IGF-ESIS.35.29